

# Hang Ke

Department of Mechanical and Aeronautical Engineering,
Clarkson University,
Potsdam, NY 13699;
Additive Manufacturing Innovations LLC,
Potsdam, NY 13676
e-mail: keh@clarkson.edu

# Alexandra Loaiza

School of Materials Engineering, Purdue University, West Lafayette, IN 47907 e-mail: yloaizal@purdue.edu

# Andres G. Jimenez

Department of Mechanical and Aeronautical Engineering, Clarkson University, Potsdam, NY 13699 e-mail: garciaji@clarkson.edu

# David F. Bahr

School of Materials Engineering, Purdue University, West Lafayette, IN 47907 e-mail: dfbahr@purdue.edu

### **Ioannis Mastorakos**

Department of Mechanical and Aeronautical Engineering, Clarkson University, Potsdam, NY 13699 e-mail: imastora@clarkson.edu

# A Multiscale Simulation Approach for the Mechanical Response of Copper/Nickel Nanofoams With Experimental Validation

Metallic nanofoams, cellular structures consisting of interlinked thin nanowires and empty pores, create low density, high surface area materials. These structures can suffer from macroscopically brittle behavior. In this work, we present a multiscale approach to study and explain the mechanical behavior of metallic nanofoams obtained by an electrospinning method. In this multiscale approach, atomistic simulations were first used to obtain the yield surfaces of different metallic nanofoam cell structures. Then, a continuum plasticity model using finite elements was used to predict the alloy nanofoam's overall strength in compression. The manufactured metallic nanofoams were produced by electrospinning a polymeric non-woven fabric containing metal precursors for alloys of copper-nickel and then thermally processing the fabric to create alloy metallic nanofoams. The nanofoams were tested with nanoindentation. The experimental results suggest that the addition of nickel increases the hardening of the nanofoams. The multiscale simulation modeling results agreed qualitatively with the experiments by suggesting that the addition of the alloying can be beneficial to the hardening behavior of the metallic nanofoams and helps to isolate the effects of alloying from morphological changes in the foam. This behavior was related to the addition of solute atoms that prevent the free dislocation movement and increase the strength of the structure. [DOI: 10.1115/1.4051806]

Keywords: mechanical behavior, microstructure property relationships, plastic behavior

## 1 Introduction

Metallic nanofoams' properties are quite different from their bulk counterparts due to their high surface-to-volume ratio and low relative density, making them excellent materials for a wide range of applications. One of the most widely studied methods to fabricate metallic nanofoams is dealloying [1], also known as the selective leaching method. One element from an alloy is removed via corrosion processes. Previous research has shown its potential to fabricate these metallic nanofoams with relatively high surface area [2–5]. However, this method has several drawbacks. First, the material choice is limited in the dealloying process since it relies on the difference of electrochemical potential between the two elements; one element will remain in the porous structure if it is more inert, and the other ingredients must be leached out from the system. Also, the relative densities of the dealloyed metallic nanofoams are generally limited between 15% and 30%. Finally, the dealloying method makes compositional strengthening mechanisms such as precipitation hardening and solid solution strengthening difficult, if not impossible.

An alternative method to create metallic nanofoam structures is using a combination of electrospinning and thermal treatments. This method enables alloys to be formed in the metallic nanofoam morphology regardless of their electrochemical potential difference [6]. This current study chose to utilize the thermochemical decomposition of two precursors dissolved in the polymeric foam template

Contributed by the Materials Division of ASME for publication in the JOURNAL OF ENGINEERING MATERIALS AND TECHNOLOGY. Manuscript received February 23, 2021; final manuscript received July 11, 2021; published online August 3, 2021. Assoc. Editor: David Field.

created by the electrospinning process. In this way, the composition is controlled by the chemistry of the template.

Metallic nanofoams often exhibit brittle behavior macroscopically due to localized plastic deformation in individual ligaments [7]. This lack of macroscopic strength is one of the limiting factors preventing their broad application. Both experimental [6] and computational [8,9] examinations of the nanoscale strengthening mechanisms have been carried out to identify ways in which the metallic nanofoams may deviate from the classic Gibson and Ashby model [10], developed to relate a foam's yield and ultimate tensile strength to the bulk solid using the relative density of the macroscopic material. However, this model fails to consider the nanostructural parameters of ligaments constituting the metallic nanofoam. The properties of the individual ligaments may have size-dependent plasticity parameters that lead to higher than predicted strength. As Hodge et al. reported [11], the bulk yield strength of metallic nanofoams varies with the ligament diameter. A modified scaling equation was proposed, which incorporates the ligament low densities and size effects.

Moreover, Fan and Fang [12] extended Hodge's model for gold nanofoams at higher relative density, and Xia et al. [13] studied the surface effects on the effective mechanical behavior of nanofoam materials by a size-dependent Timoshenko nanobeam model. Feng et al. [14] examined the surface effect on the effective Young's modulus of open-cell nanofoams by adding a surface layer into the unit-cell micromechanics model. The scaling laws that tie metallic nanowires to metallic nanofoams have been refined by Briot and Balk [15].

Overall, metallic nanofoams' mechanical behavior is determined by the relationship between the individual ligaments' behavior, of which this material is formed, and their geometry. Most reported computational work on foams is focused either on the mechanical behavior of the nanoligaments or on simplified geometrical models that neglect the atomistic configurations [10]. Our previous work [16,17] investigated the macroscopic mechanical behavior of copper and composite copper/nickel nanofoams under compression using a combination of molecular dynamics and finite elements.

The present work aims to expand the previous work to study copper/nickel alloy nanofoams and investigate how the geometry and composition affect their macroscopic mechanical behavior. We also address the issue of strengthening individual ligaments with a parallel understanding of foam morphology. We used experimental results to identify proper simulation geometries and simulations to validate and explain the experimental findings.

In our approach, molecular dynamics (MD) simulations were performed in several representative cell structures to obtain their yield points for complex load conditions under compression. These yield points were then curve fitted to a theoretical model [18] to obtain yield surfaces. These yield surfaces were then used in a plasticity continuum model [19] to simulate the macroscopic compressive behavior of the alloyed nanofoams. Finally, these results were compared with Cu/Ni alloy nanofoams fabricated using the electrospinning method mentioned earlier.

#### 2 Methodology

In this section, we describe the experimental procedure and simulation methodologies we are using in this work. Three structures we considered, more specifically, pure Cu, 10 wt% Ni–90 wt% Cu, and 50 wt% Ni–50 wt% Cu. The choice of the particular nanofoams was made based on three factors: (a) the availability of reliable interatomic potentials for the molecular dynamics simulations, (b) the importance of copper and nickel in many potential metallic nanofoam applications, and (c) to demonstrate the capability of the employed manufacturing process to produce nanofoams of any metal.

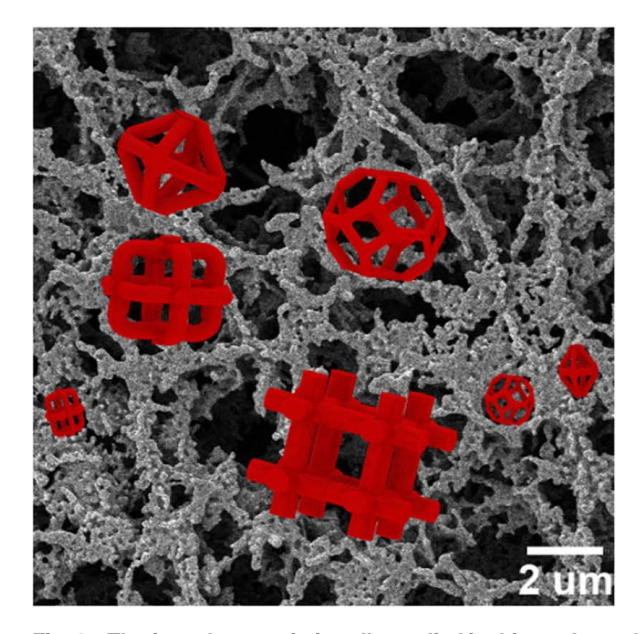
**2.1 Experimental Procedure.** Cu and Cu/Ni metallic nanofoams were created by an electrospinning polymer templating technique [20]. The process to develop foams of pure Cu and Cu/Ni used polyvinyl alcohol (PVA) with an average molecular weight

of 146,000-186,000, 87-89% hydrolyzed) as a polymer carrier for metallic salts (Copper (III) acetate monohydrate, Acros Organics; Ni (II) acetate tetrahydrate 98%, Sigma Aldrich; zinc acetate dihydrate, Fluka Analytical). Metallic salts (Cu and Cu/Ni) at a different mass ratio from 0 wt% to 50 wt% were blended with a magnetic stirrer for 12 h at room temperature with Deionized (DI) water and glacial acetic acid (99.7–100.5%, British Drug Houses (BDH) Chemicals) in a 1:1:1 mass ratio. Acetic acid was added to avoid clogging at the tip of the needle in the electrospinning process. The resulting solution was then mixed with a 10 wt% PVA solution in a different mass ratio from 2 wt% to 8 wt%, which was previously magnetically stirred for 12 h at room temperature to control the viscosity of the precursor solution and then stirred for an additional 12 h. The precursors' viscosity was assessed using a Bohlin Gemini rheometer (Malvern Instruments, UK) at room temperature and cone and plate fixture with a diameter of 40 mm in the top rotational plate with 500- $\mu$ m gap. The shear rate was increased from 0.01 to 215 s-1 and the viscosity value reported here is at 0.03 s<sup>-1</sup>, which is the shear rate through the needle used. The shear rate was found using the equation developed by Blair et al.

$$\gamma = \frac{4Q}{\pi R^3} \tag{1}$$

In Eq. (1),  $\gamma$  is the shear rate, Q volumetric flowrate, and R is the needle's radius.

Precursors were electrospun using a 12-cm distance between a copper foil working as a collector (cathode) and a 19 gauge stainless-steel needle (anode) connected through a power supply applying a voltage of 15 keV. The volume flowrate for the electrospinning process was kept at 0.07 mL/h. The sample was pyrolyzed/calcinated in the air at 500 °C; the soak temperature was reached using a heating rate of 5 °C/min. The sample was soaked at temperature for two hours, and then, the furnace cooled to room temperature. After the calcination process, the remaining CuO was transferred to an infrared furnace for a reduction heat-treatment process. The sample is heated to 300 °C for 30 mins while purging with a flowing reducing gas atmosphere (5% H<sub>2</sub>, 95% Ar). After this process, the sample has a metallic nanofoam



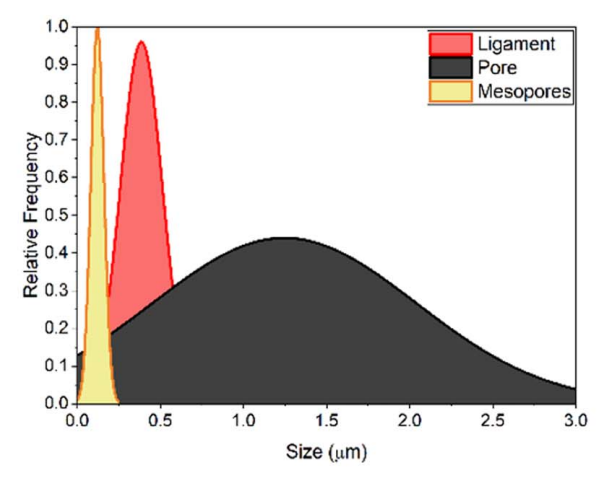


Fig. 1 The four characteristic cells studied in this work overlayed the microstructure of a typical nanofoam used in this study (pure Cu in this example). Scale bar 2  $\mu$ m. The distribution of pore diameter, ligament size, and mesopores (present within a ligament) show that the average diameter of the ligaments is 390 nm, the average size of pores is 1250 nm, and the average mesopore size is 120 nm.

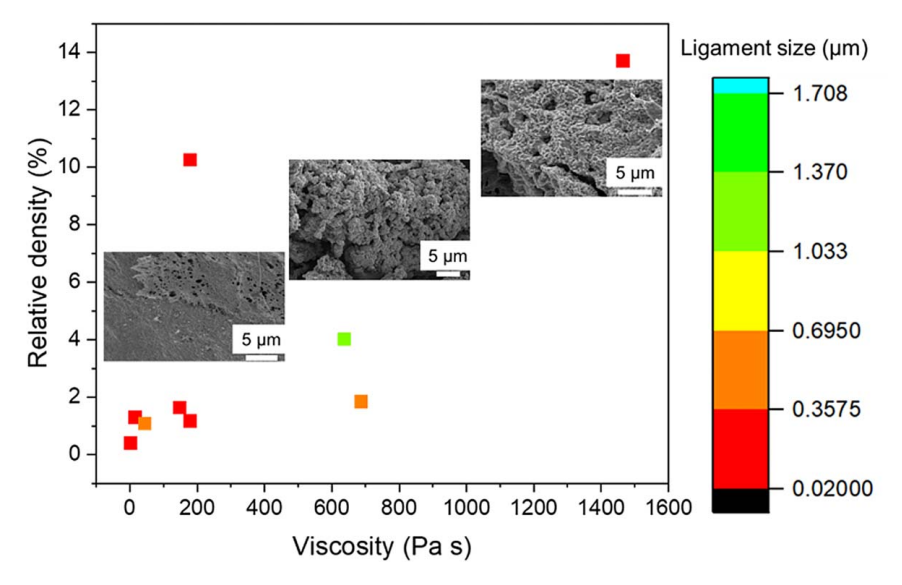


Fig. 2 The relative density and ligament size of Cu and alloy nanofoam after all thermal processing as a function of precursor viscosity

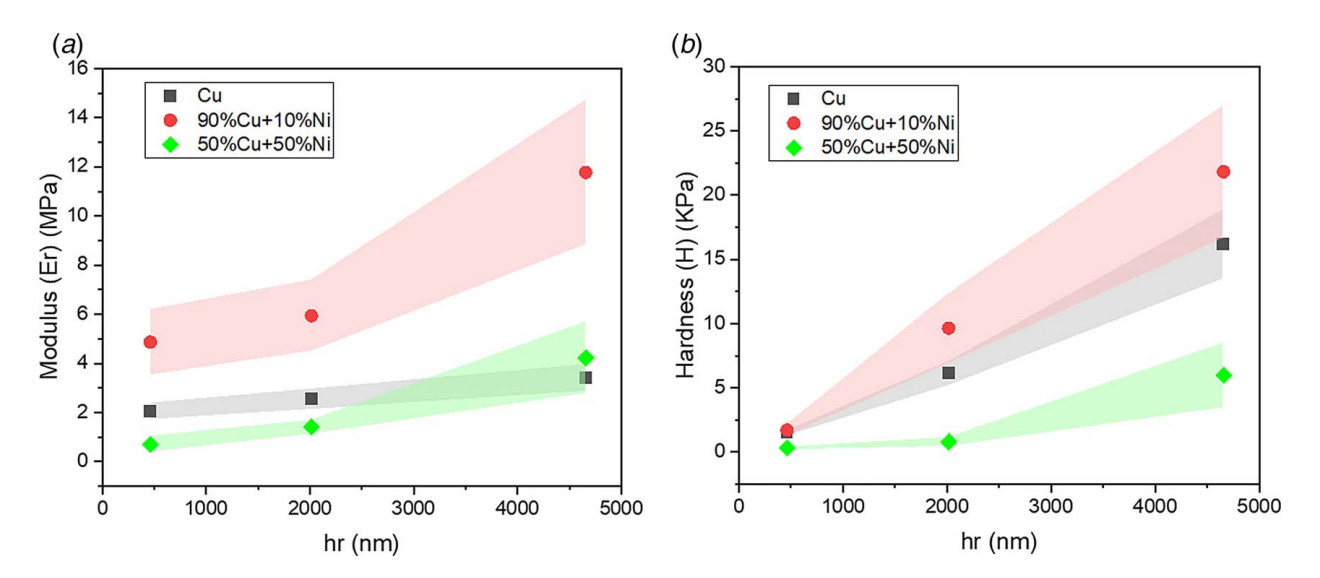


Fig. 3 Experimentally measured mechanical properties of Cu and Cu–Ni alloys using flat punch indentation. (a) Er (MPa) for Cu alloy with 10 and 50 wt%Ni. (b) H (kPa) for Cu alloy with 10 and 50 wt%Ni. The relative densities and ligament sizes of the Cu and Cu–10 wt%Ni foams were similar, and the density and ligament size of the 50/50 nanofoam was lower than the other two conditions.

structure. Relative density and ligament size measurements were taken for samples made with different viscosity.

#### 2.2 Multiscale Simulations

2.2.1 Nanofoam Cell Structure Generation. First, several types of cell structures have been created to mimic the porous characteristic of metallic nanofoams. Previous studies have used various techniques to generate the metallic nanofoam structure. For example, Gunkelmann et al. [22,23] and Ke et al. [17] created the nanofoams from a perfect face-centered cubic (FCC) crystal with periodic boundary conditions that were then heated above the melting temperature. The metallic nanofoams have been obtained by removing the atoms with temperatures above a determined value explicitly chosen to get the desired porosity. Crowson et al. introduced a phase-field model to create gold nanofoams through the spinodal decomposition of a binary alloy. Their samples showed similar atomistic configurations with real experimental findings in terms of ligament size distribution and surface curvature. An alternative method uses

atomistic Monte Carlo (MC) simulations of binary mixtures to generate metallic nanofoams by spinodal decomposition. All the above techniques produced random nanofoam structures with relative densities in the range of 40%–60%. The ratio of the number of atoms of the foam over the number of particles of the bulk material occupying the same volume defines the relative density. Due to their randomness, these structures cannot provide information about the effect of nanoligament connectivity and nanofoam local geometry on the strengthening of the nanofoams. To resolve this issue, in this work, we propose a different approach. Instead of creating random structures, we generated geometric structures representing ordered periodic nanofoam cells like these suggested in Ref. [10], with minor modifications and differentiation to obtain the desired total number of ligaments linked to joints. Here, we continue to use the nanofoam cell structures shown in Ref. [16]. Based on the specific geometric characteristics, each foam cell possesses certain mechanical properties. A random nanofoam can then be modeled as a random distribution of geometric cells like those we consider in this paper. A specific mechanical property, such as the nanofoam

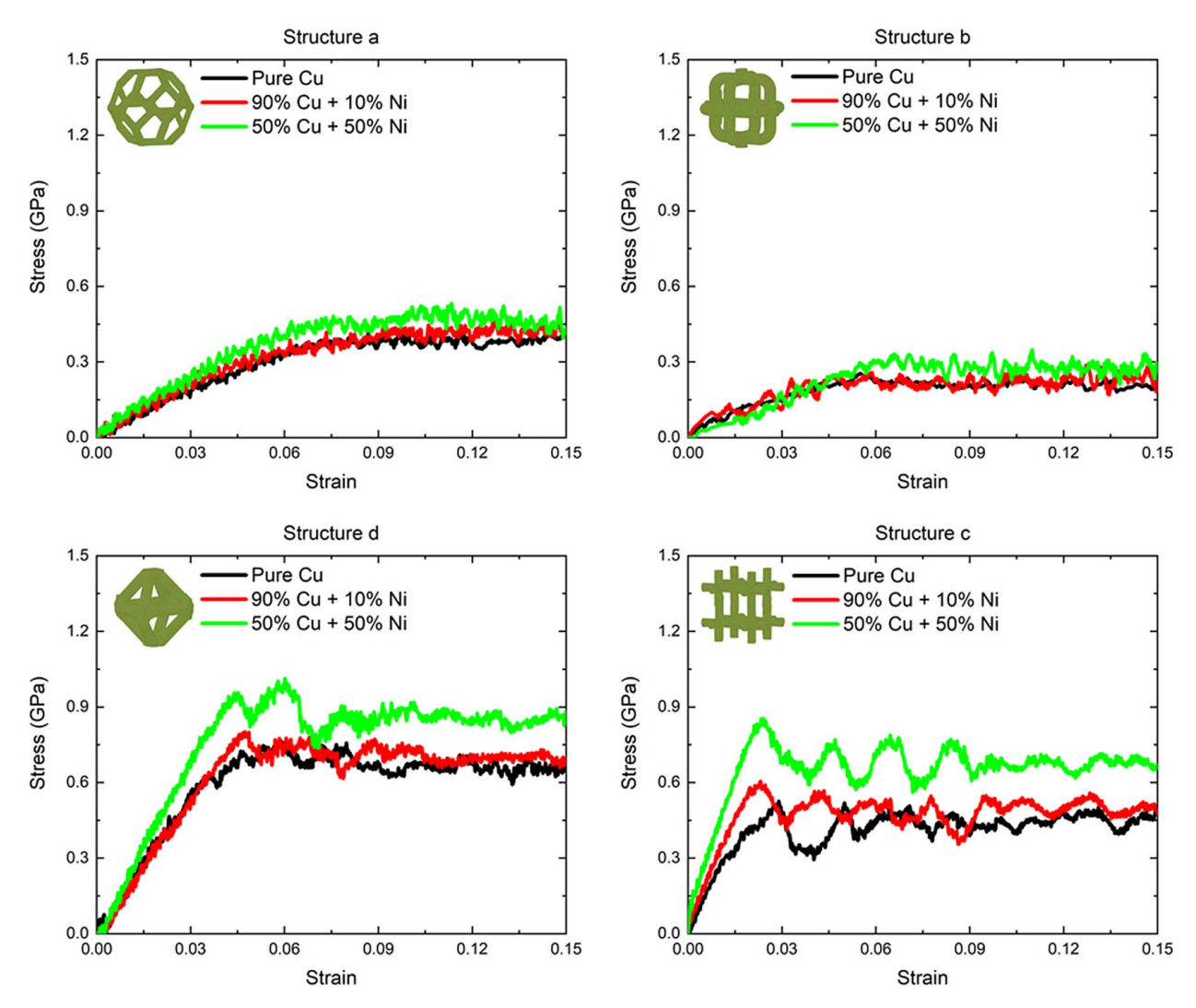


Fig. 4 The stress–strain curves of the four types of structures during uniaxial compression. The shape of each structure is shown in the top left corner. The lower lines represent the pure Cu structures, the mid lines represent the  $Cu_{90}Ni_{10}$  alloy structures, and the top lines represent the  $Cu_{50}Ni_{50}$  alloy structures.

strength, should fall within the range defined by the minimum-maximum strengths of the ordered nanofoams made with geometric representative cell structures. The geometric cell shapes have been obtained from the experimental specimens' characterization in this work, as shown in Fig. 1, where the cell shapes are overlayed on a micrograph of the pure Cu nanofoam. A distribution plot of pore sizes and ligament diameter is shown for this particular nanofoam; the relative dimensions of pores, ligament diameters as shown in Fig. 1 are similar for all three materials.

Of course, the random and heterogeneous nature of the metallic nanofoam cannot be represented precisely by an ordered unit-cell geometry like the one we suggest in this paper. On the other hand, creating a completely random nanofoam in molecular dynamics represents a challenge. The small length scale prevents a large range of heterogeneities, resulting in more homogeneous nanofoams with a random pore distribution. The approach we are presenting in this paper is a compromise to allow the study of random metallic nanofoams with various pores sizes and shapes. This paper represents the first attempt with only a few possible unit cells in an actual metallic nanofoam. More unit cell types must be included for a more representative analysis, as the number, varieties, and sizes of cells that can be identified are very large. Despite that, even a small number of cells, like the ones we use herein, can be enough to demonstrate the validity of the methodology as it will be shown.

A simulation box consisting of  $150\times150\times150$  copper atoms with (001) direction was formed. For the pure copper nanofoams, the radius of the individual ligament was kept at 3 nm for all the cases. For the alloyed Cu/Ni nanofoams, 10 wt% Ni–90 wt% Cu and 50 wt% Ni–50 wt% Cu were studied. Also, to consider the size effect involved in our current research, we decrease our simulation box size to 75% and 50% of its original box size.

2.2.2 Molecular Dynamics Simulations. The purpose of the molecular dynamics simulations in this paper is to gain more insight into the nanofoam ligaments' deformation mechanisms and understand how these mechanisms are related to the mechanical behavior of the manufactured nanofoams. As the average thickness of the experimentally tested nanofoam ligaments was at  $\sim$ 750 nm, justifying the term nanofoams, this is outside the molecular dynamics capabilities. Therefore, we choose to perform simulations on metallic nanofoams of similar porosity with the experimental ones by sizing down the cell and ligaments size of the simulated ones. Although this approach will affect the quantitative results, producing much yield stresses, it will preserve the general trends related to the effect of the various geometry and material parameters, thus providing qualitative results that can be compared to the experimental findings. Our view is that the manufacturing of metallic nanofoams with thinner ligaments will be possible in the future. Therefore, the

Table 1 Relative density, uniaxial compressive yield strength, and the parameter  $\alpha$  of different types of cell structures

Structure name	Material composition	Relative density (%)	Uniaxial yield strength (GPa)	Alpha (α)
a1	100% Cu	6.97	0.418	0.535
a2	90% Cu + 10% Ni	6.97	0.396	0.345
a3	50% Cu + 50% Ni	6.97	0.481	0.372
b1	100% Cu	12.25	0.251	1.104
b2	90% Cu + 10% Ni	12.25	0.259	0.836
b3	50% Cu + 50% Ni	12.25	0.323	0.879
c1	100% Cu	10.06	0.426	1.272
c2	90% Cu + 10% Ni	10.06	0.602	1.082
c3	50% Cu + 50% Ni	10.06	0.854	1.370
d1	100% Cu	10.87	0.763	0.645
d2	90% Cu + 10% Ni	10.87	0.802	0.547
d3	50% Cu + 50% Ni	10.87	1.002	0.563

choice of molecular dynamics method used in this study and the subsequent findings is further justified.

The simulations were performed using Large-scale Atomic/ Molecular Massively Parallel Simulator (LAMMPS) [24] with the embedded atom method (EAM) [25,26]. The Voter and Chen [27] interatomic potential was used to describe the atomic interactions between Cu and Ni. Periodic boundary conditions were assumed in all three directions to model infinitely large metallic nanofoams. The temperature was kept constant to 300 K during both the relaxation and loading steps in all simulations. The isothermal-isobaric (NPT) ensemble was used to update the atomic velocities and positions at each simulation step. The cell structures were subjected to three different compressive loading conditions, uniaxial, hydrostatic, and mixed with a strain rate of  $5 \times 10^9$  s<sup>-1</sup>. The hydrostatic stress was first decreased to a fraction (3/4, 2/4, and 1/4) of the hydrostatic yield strengths for the mixed compression loading, and a uniaxial compression was applied along z-direction until yield was achieved with the hydrostatic stress in the other two directions being kept constant. Using the yield points produced by the atomistic simulations, yield surfaces were generated and curve fitted into the isotropic constitutive model suggested by Deshpande and Fleck [18] to describe the multiaxial compressive behavior of nanofoams. The methodology used is similar to that described in detail in Refs. [16,17].

#### 3 Results and Discussions

**3.1** Experimental Findings. The resulting microstructure of metallic nanofoam was investigated, as shown in Fig. 2. The relative density is increasing as the viscosity of the precursor increases for nanofoams at similar ligament sizes. The scale color on the right side indicates the average ligament sizes of the different samples on the plot. As shown in Fig. 2, the final relative density is more affected by precursor viscosity than ligament size; however, it seems that it may also contribute to the total relative density. This increase in relative density could be attributed to weaker bonds between PVA water when PVA quantity is small compared to PVA–PVA bonds when more PVA is added to the mixture to make it more viscous. The SEM images at different precursor viscosity show a denser microstructure and thicker ligament sizes as the precursor viscosity is higher.

Nanoindentation was carried out on a Hysitron Triboindenter 950 using a flat punch probe with a diameter of  $100 \,\mu\text{m}$ . Twenty-five indentations were made in in-depth control mode to a maximum depth of 4700 nm in three loading–unloading cycles. Figure 3 presents the average reduced modulus and hardness obtained on the pure Cu,  $10 \,\text{wt}\%\text{Ni}$ – $90 \,\text{wt}\%\text{Cu}$ , and  $50 \,\text{wt}\%\text{Ni}$ – $50 \,\text{wt}\%\text{Cu}$  alloys. Modulus and hardness of Cu with the additions  $10 \,\text{wt}\%$  Ni increased up to 243% and 59%, respectively. The shades on the plots indicate the standard error. The general trend of increasing hardness and modulus with increasing depth suggests densification and possibly buckling effects on the sample [28,29].

The observed increase in modulus and strength at any given depth (strain) in the 10% Ni alloy films confirms the hypothesis that alloying can be used to manufacture stronger (and stiffer) nanofoams. However, the sample that contains 50 wt% Ni does not show the expected behavior. The relative density of the samples studied ranges from 1.6% to 4.2%, and ligament sizes are between  $0.3\,\mu\text{m}$  and  $1.2\,\mu\text{m}$ , a significant variation across the samples (with the smaller ligaments corresponding to the higher Ni alloying fraction). Microstructural differences and foam morphology are not negligible, and they play an essential role in the final mechanical properties. Therefore, it is necessary to consider simulations in which these effects can be isolated. Previous studies have shown

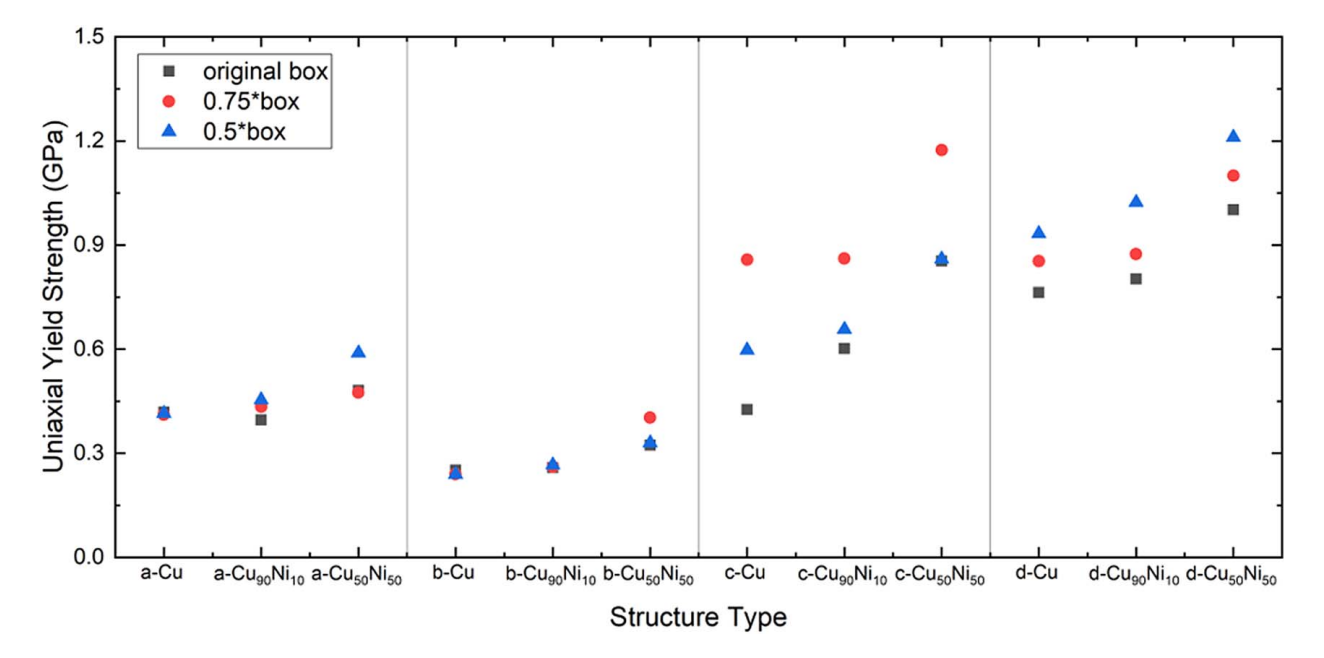


Fig. 5 Comparison of the yield strengths of each structure type and different box sizes. The original box, 0.75\*box, and 0.5\*box are shown with square, circular, and triangular marks, respectively.

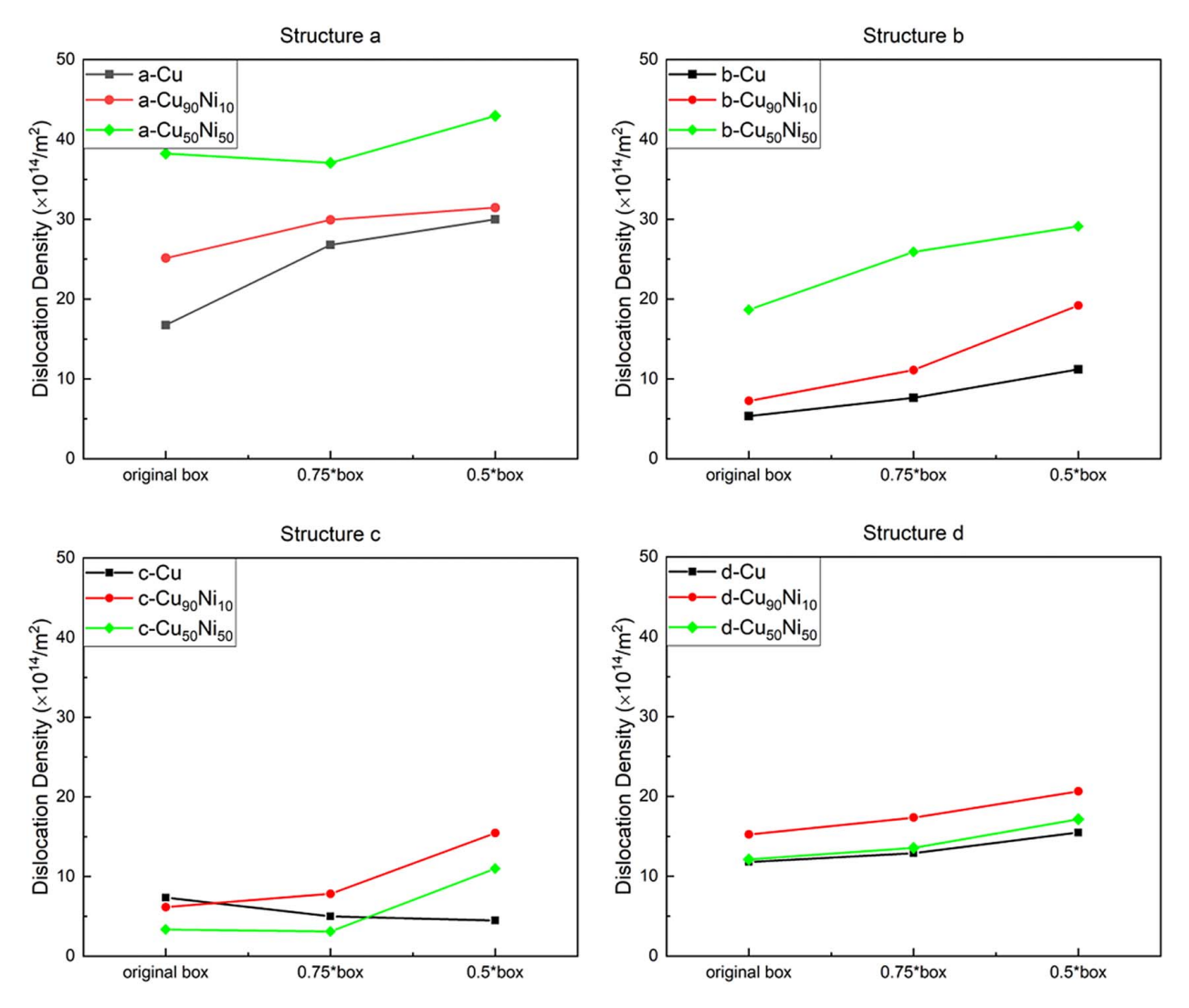


Fig. 6 The dislocation density for different cell structures and different box sizes. Here, we calculate the dislocation density right after the yield point is reached for each structure. It is the ratio of total dislocation length to the total volume.

that nanoindentation properties could be tailored by modifying the structural factors, such as ligaments and pores sizes and structural disorder [30].

#### 3.2 Simulation Results

3.2.1 Stress-Strain Curves. Our previous study [16] examined the effect of a core-shell (Cu-Ni) layered composite but did not

capture the impact of the more common (and experimentally more accessible) solid solution strengthening mechanism. Figure 4 shows the stress–strain curves under uniaxial compression for the pure Cu structures and Cu/Ni alloy structures, and Table 1 lists the yield strengths and the relative density of each system. While comparing nanoindentation results with uniaxial compression is challenging, particularly in these random structures, the size of the flat tip used in the nanoindentation in the experiment

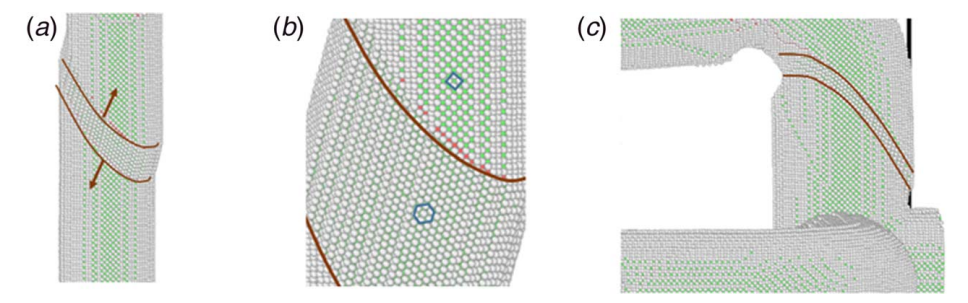


Fig. 7 (a) A part of the perpendicular ligament of structure c during uniaxial compression loading along the main axis of the ligament. The twin boundaries and their propagation are shown with the straight lines and arrows, respectively. (b) The structure transformation from <001>/{100}(the rectangle on top) to <110>/{111} (the hexagon shape). (c) The same behavior on structure b during mixed biaxial loading.

Table 2 Parameter used for different types of structures in the finite element method (FEM) analysis to simulate the macroscopic compressive behavior of pure Cu and Cu/Ni alloy nanofoams

	α2 (MPa)	β	γ (MPa)	E (MPa)	Yo (MPa)	eD	α
a-Cu	12.70	3.07	12.69	602	10.0	0.9303	0.535
a-Cu <sub>90</sub> Ni <sub>10</sub>	12.70	3.07	12.69	643	10.1	0.9303	0.345
a-Cu <sub>50</sub> Ni <sub>50</sub>	12.70	3.07	12.69	804	10.7	0.9303	0.372
b-Cu	12.78	2.12	12.76	1861	23.0	0.8775	1.104
b-Cu <sub>90</sub> Ni <sub>10</sub>	12.78	2.12	12.76	1986	23.2	0.8775	0.836
b-Cu <sub>50</sub> Ni <sub>50</sub>	12.78	2.12	12.76	2484	24.6	0.8775	0.879
c-Cu	12.75	2.47	12.74	1255	17.5	0.8994	1.272
c-Cu <sub>90</sub> Ni <sub>10</sub>	12.75	2.47	12.74	1340	17.7	0.8994	1.082
c-Cu <sub>50</sub> Ni <sub>50</sub>	12.75	2.47	12.74	1675	18.7	0.8994	1.370
d-Cu	12.76	2.33	12.75	1465	19.6	0.8913	0.645
d-Cu <sub>90</sub> Ni <sub>10</sub>	12.76	2.33	12.75	1563	19.8	0.8913	0.547
d-Cu <sub>50</sub> Ni <sub>50</sub>	12.76	2.33	12.75	1956	21.0	0.8913	0.563

ensures 100's to 1000's of ligaments will be probed, and as such should scale with macroscopic compression. Of course, a direct comparison is not possible, but we used this methodology to systematize the simulation of random nanostructures, and this paper should be viewed as the first step toward a more quantitative

simulation. Furthermore, although the mechanical behavior of an individual cell cannot also be compared to the collective behavior of the random nanofoam recorded in Fig. 2, the average behavior of the various nanofoam cells should be able to capture this effect, therefore providing valuable qualitative insight.

Overall, during uniaxial compression, these featured structures will undergo elastic deformations until yield. Here, we compare the yield strengths of these structures to study the strength of each structure. It is expected that the experimental specimen is a random collection of simple geometric cells of various sizes. From Table 1, the yield strength depends on both the geometry of the cell and the material type. For example, the yield strength of pure Cu structures varies from about 0.25 to 0.75 GPa. The Cu/Ni alloy structure increases the yield stress, which again depends on the structure's geometry. More specifically, the yield strength of Cu<sub>50</sub>Ni<sub>50</sub> alloys has increased 15%, 29%, 100%, and 31% for types "a," "b," "c," and "d," respectively, compared to pure Cu cell structure. The reason is that the introduction of the different-sized atoms (Ni) breaks the previous Cu crystal structure's symmetry and regularity, so they could not slide as easily as pure structures. Here, we find that the yield strength increase is more evident in the case of structure "c" compared with the other three structures, resulting from the orientation of the ligaments to the loading direction. In the structure "c," these straight perpendicular ligaments are parallel to the loading direction. They can withstand more loading before deforming

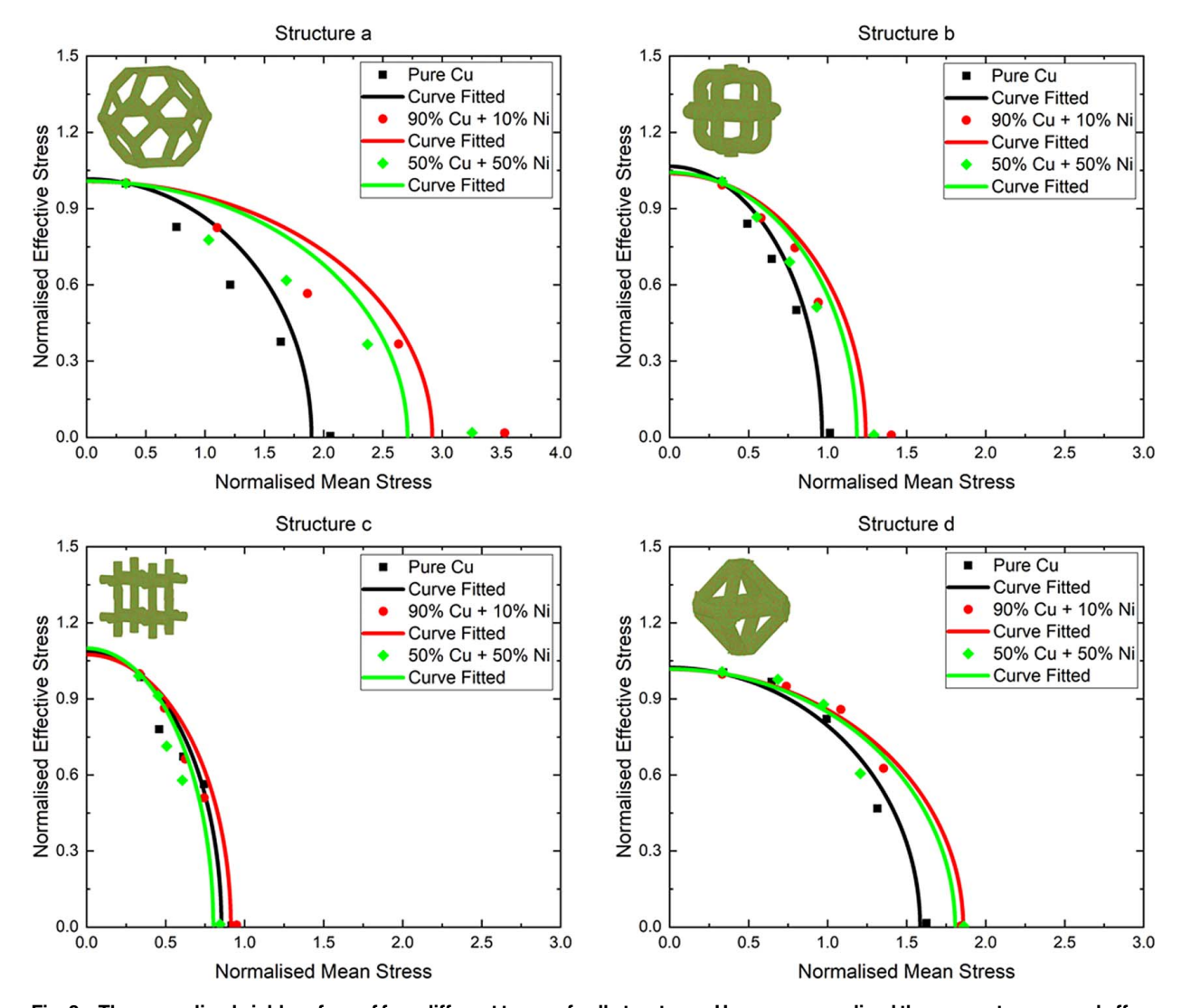


Fig. 8 The normalized yield surface of four different types of cell structures. Here, we normalized the mean stresses and effective stresses by the uniaxial compressive yield strength.

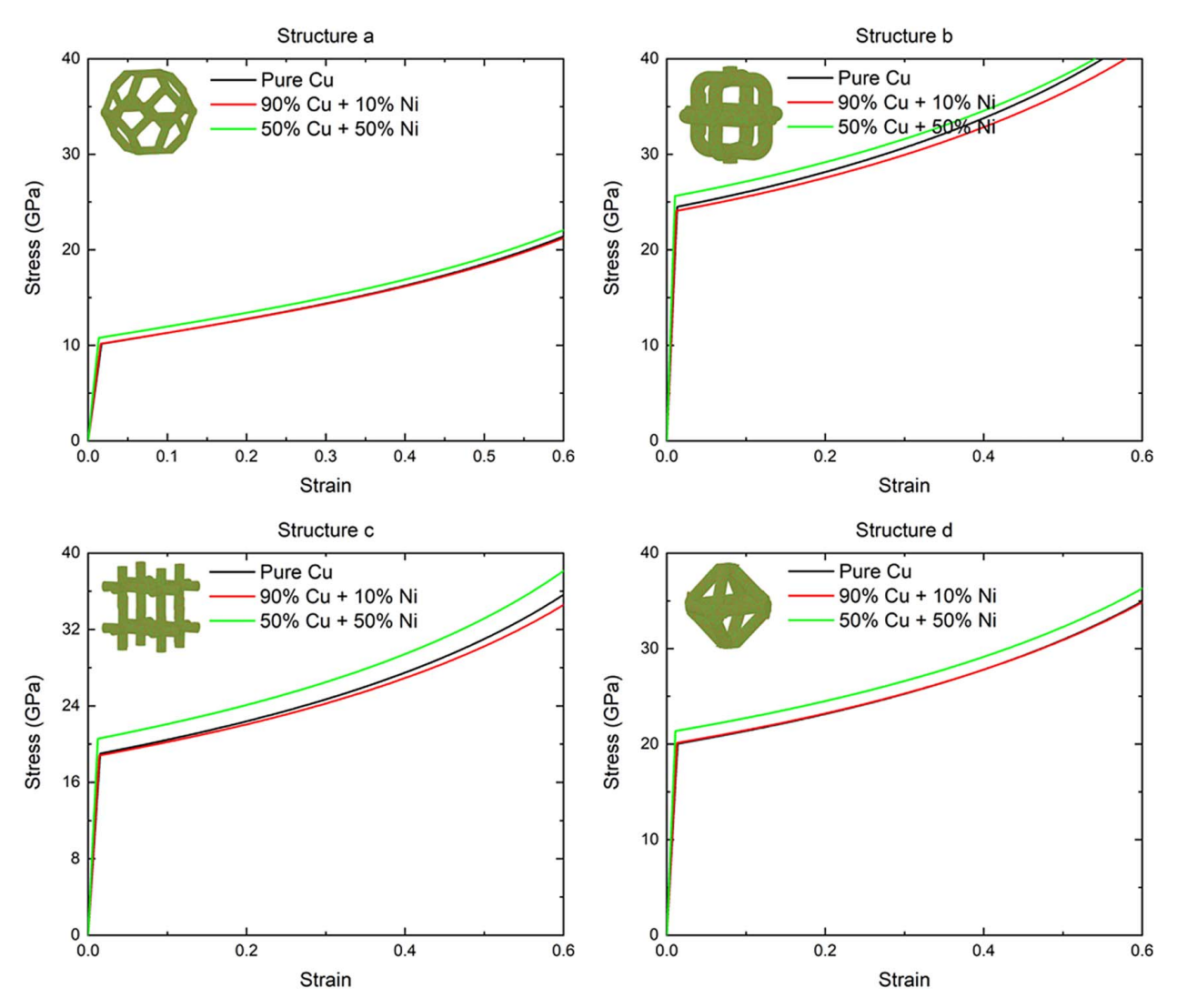


Fig. 9 Macroscopic stress-strain curves for the four types of pure Cu and Cu/Ni alloy nanofoams

plastically without buckling. Simultaneously, the other structure types have ligaments angled to the loading direction, and they exhibit some buckling before they deform plastically.

Figure 5 compares the uniaxial yield strength of the Cu and Cu/Ni alloy nanofoams at different simulation box sizes. It is seen from Fig. 5 that the yield strengths increase with the reduction of box size and alloying in general agreement with the experimental results. As we mentioned before, we changed the box size in molecular dynamics simulations while keeping the same porosity; therefore, the ligament size has changed accordingly, suggesting a Hall-Petch type of strengthening, a standard strengthening method in metals when the average grain size decreases. In our case, the ligament plays the role of the grains, and because the radius of the ligaments has decreased, the overall strengths increased.

As we are primarily interested in recording trends, e.g., the effect of solute atoms in pure copper nanofoams and how that improves the mechanical properties as shown in experiments, we did not do an extensive box-size convergence analysis. However, such an analysis is premature at this point, since the change in box size will change the quantitative results and not the overall qualitative trend that is of interest.

Another way to explain the strengthening effect is by using the dislocation density inside the cells, shown in Fig. 6. The results suggest that solute atoms increase the initial dislocation density in some structures, while in others do not affect it or even decrease it. This indicates that the mechanism responsible for strengthening the alloyed structures is not related to the nature of the alloy that

favors the production of more dislocations but rather to the inclusion of solute atoms acting as barriers to the alloy dislocation motion. Furthermore, the dislocation density within these structures increases as the box size reduces, making the dislocation more challenging to slide and increasing overall strength. These curves are compared well to the experimental ones in Fig. 3, showing a similar trend. Combining alloying elements with a small ligament size leads to higher dislocation densities that result in increased strength. The range of dislocation densities for the various compositions and box sizes (e.g., ligament sizes) agrees with the experimental observation in Fig. 3. The foam morphology plays an essential role in the final mechanical properties. Although this happens in both pure and alloyed nanofoams, it is more evident in the alloyed structure due to the higher dislocation density than the pure copper ones.

3.2.2 Ligament Behavior During Compression. The individual ligaments' deformation behavior showed dependence on the orientation of the individual ligament to the loading direction. Unit cells like structures b and c with straight perpendicular ligaments showed the deformation behavior related to the nucleation and propagation of multiple twin boundaries during compression, as shown in Fig. 7(a). During the compression, the original ligament configuration of  $<001>/\{100\}$  is transformed to ligaments with mixed configurations of  $<001>/\{100\}$  and  $<110>/\{111\}$  (Fig. 7(b)). This transformation has been shown in metallic nanowires [31] and alters the ligaments' mechanical behavior during removing loading, resulting in pseudoelasticity [32,33]. In small ligament

thicknesses (below 2–3 nm at 300 K), this process can lead to the complete recovery of the original ligaments. In thicker ligaments, the process cannot be reversed completely, resulting in partial recovery. All ligaments in all structures exhibited this behavior, although it was more intense in structures b and c with perpendicular ligaments. The twin zone thickness (the zone between the two twin boundaries) depended on the ligaments' size and relative orientation to the loading direction. During mixed loading, the twin zone thickness was smaller (Fig. 7(c)), suggesting that only the perpendicular component of the loading contributes to the twinning. This behavior can explain the partial recovery detected during the compression of metallic nanofoams and can be exploited to improve the nanofoam properties. However, the further analysis required to understand this effect and its limitations better is beyond this paper's score and will be addressed in a separate work.

3.2.3 Plasticity Model. The plasticity model requires a description of the yield surfaces and the hardening of the nanofoams. The yield surfaces [34] for the four structures were calculated from the stress-strain curves of the four-unit structures using molecular dynamics. We conducted five compression tests for each structure, including a pure uniaxial compression, a pure hydrostatic compression, and three combinations of hydrostatic and uniaxial compressions per the previous section's methodology. To curve fit the produced yield points to the theoretical model, the mean and effective stresses must be normalized with the uniaxial compressive yield strength for each case, as listed in Table 2. Figure 8 shows the normalized yield points and the resulting normalized yield surfaces. We must also note that for the uniaxial compression yield point in all structures, the normalized mean stresses are 1/3, and the normalized effective stresses are 1.0. The high strain rates result in higher yield stresses, but the normalization allows the implementation of this yield function even for this case. The normalization of the yield stress used in this model makes it very suitable for its application with the molecular dynamics results that incorporate much higher strain rates than actual experiments.

The obtained parameters from the normalized yield surfaces were then used as in Ref. [17]. The plastic behavior was described using the following hardening functions [19]

$$Y = Y_o + \gamma \frac{\hat{\varepsilon}}{\varepsilon_D} + \alpha_2 \ln \left( \frac{1}{1 - (\hat{\varepsilon}/\varepsilon_D)^{\beta}} \right)$$
 (2)

where the phenomenological parameters  $\alpha_2$ ,  $\gamma$ , and  $\beta$  depend on the relative density of the foam

$$\left\{\alpha_2, \gamma, \frac{1}{\beta}\right\} = C_0 + C_1 \left(\frac{\rho_f}{\rho_o}\right)^n \tag{3}$$

with  $C_0$ ,  $C_1$ , and n constants determined by fitting experimental data on Cu nanofoams during compression [35]. The validity of this model has already been shown in the previous work [16].

The elastic modulus of the pure Cu nanofoam was determined using the scaling equation [10]

$$E = E_o \left(\frac{\rho_f}{\rho_o}\right)^2 \tag{4}$$

where  $E_o$  is the elastic modulus of bulk Cu. We used the general rule of mixtures like in Ref. [6] for the different structures for the alloy nanofoams.

3.2.4 Macroscopic Stress-Strain Curves for Cu Nanofoams. Table 2 lists the parameters required for the FEM of each structure, as obtained by the previous paragraph's methodology for all cell arrangements. The simulated stress-strain curves of the pure Cu and Cu/Ni alloy nanofoams are shown in Fig. 9. The results suggest that the introduction of nickel atoms slightly improves the mechanical behavior of metallic nanofoams. The improvement depends on the geometry of the unit cell structure we consider. The results represent the mechanical behavior of ordered metal

nanofoams since the same unit structure is repeatedly used in every integration point. In random nanofoams, this will not occur, as the geometry and the relative density could vary at every integration point. Therefore, a random nanofoam's macroscopic stress at every strain will fall within the minimum and maximum value of stress in this strain point of all structures. In this view, a random metallic nanofoam can be approximated as a collection of all the unit cell geometries randomly distributed inside the macroscopic structure. In general, these ranges of stress calculated from our simulations, as shown in Fig. 9, are in good agreement with the experiment results.

#### 4 Conclusions

By comparing experimental solid solution alloys in a metallic nanofoam geometry with a multiscale model of the deformation of the foam in compression, we demonstrate the extent to which solid solution strengthening can impact the yield of the metallic nanofoam structure. Four specific types of cell structures have been constructed based on the characterization of the experimental specimens. The cell structures were distinguished by the number of ligaments connected to one joint. The yield surface of these structures was generated using molecular dynamics, and the results were implemented into a yield equation that incorporated both the mean and effective stresses. Furthermore, the molecular dynamics simulations revealed a twin boundary propagation mechanism during the compression that may be responsible for any partial recovery of the metallic nanofoams during unloading. Also, finite element simulations have been implemented to study the Cu nanofoams' macroscopic mechanical behavior under a uniaxial compression test. Overall, for a given morphology, the alloyed nanofoams were stronger than their pure copper counterparts under compression. This behavior was attributed to the inclusion of the nickel atoms in the copper metal matrix that provided increased resistance to the dislocation motion. That resulted in a higher dislocation density inside the alloyed ligaments, as fewer dislocations were now free to move to the free surface, and thus an increase in strength. However, the experiments suggest that this trend is not uniform. Changes in the nanofoams' morphology (connectivity and spacing) can lead to strength and stiffness decrease for the highest alloy concentrations. The nanofoam morphology deviates the highest from the pure Cu and lower alloy (10 wt% Ni) nanofoam. Structural factors such as ligament diameter and pore size may cause a more dominant effect on the resulting properties than a solid solution effect. When the chemistry of the nanofoam is modified in the precursor, structural factors such as ligament size and relative density are modified as well. This is likely the cause of the experimentally observed reduction in strength of the nanofoam with the highest alloy content studied here (50 wt% Ni).

#### Acknowledgment

This work was supported by the National Science Foundation under Grant Nos. CMMI-MEP-1634640 and CMMI-MEP-1634772. Some of the computing for this project was performed on the ACRES cluster, funded by the National Science Foundation under Grant No. 1925596. HK, AGJ, and IM would like to thank the NSF and Clarkson University's Office of Information Technology for providing computational resources and support that contributed to these research results.

#### References

- [1] Stratmann, M., and Rohwerder, M., 2001, "A Pore View of Corrosion," Nature, 410(6827), pp. 421–423.
- [2] Erlebacher, J., Aziz, M. J., Karma, A., Dimitrov, N., and Sieradzki, K., 2001, "Evolution of Nanoporosity in Dealloying," Nature, 410(6827), pp. 450– 453.

- [3] Katagiri, A., and Nakata, M., 2003, "Preparation of a High Surface Area Nickel Electrode by Alloying and Dealloying in a ZnCl<sub>2</sub> NaCl Melt," J. Electrochem. Soc., 150(9), pp. C585–C590.
- [4] Sun, Y., and Xia, Y., 2003, "Alloying and Dealloying Processes Involved in the Preparation of Metal Nanoshells Through a Galvanic Replacement Reaction," Nano Lett., 3(11), pp. 1569–1572.
- [5] Sun, L., Chien, C.-L., and Searson, P. C., 2004, "Fabrication of Nanoporous Nickel by Electrochemical Dealloying," Chem. Mater., 16(16), pp. 3125–3129.
- [6] Kim, C.-E., Rahimi, R. M., Hightower, N., Mastorakos, I., and Bahr, D. F., 2018, "Synthesis, Microstructure, and Mechanical Properties of Polycrystalline Cu Nano-foam," MRS Adv., 3(8–9), pp. 469–475.
- [7] Biener, J., Hodge, A. M., and Hamza, A. V., 2005, "Microscopic Failure Behavior of Nanoporous Gold," Appl. Phys. Lett., 87(12), p. 121908.
- [8] He, L., and Abdolrahim, N., 2018, "Deformation Mechanisms and Ductility Enhancement in Core-Shell Cu@Ni Nanoporous Metals," Comput. Mater. Sci., 150, pp. 397–404.
- [9] Abdolrahim, N., Bahr, D. F., Revard, B., Reilly, C., Ye, J., Balk, T. J., and Zbib, H. M., 2013, "The Mechanical Response of Core-Shell Structures for Nanoporous Metallic Materials," Philos. Mag., 93(7), pp. 736–748.
- [10] Gibson, L. J., and Ashby, M. F., 1997, Cellular Solids: Structure and Properties, Cambridge University Press, Cambridge, UK.
- [11] Hodge, A. M., Biener, J., Hayes, J. R., Bythrow, P. M., Volkert, C. A., and Hamza, A. V., 2007, "Scaling Equation for Yield Strength of Nanoporous Open-Cell Foams," Acta Mater., 55(4), pp. 1343–1349.
- [12] Fan, H. L., and Fang, D. N., 2009, "Modeling and Limits of Strength of Nanoporous Foams," Mater. Des., 30(5), pp. 1441–1444.
- [13] Xia, R., Li, X., Qin, Q., Liu, J., and Feng, X.-Q., 2011, "Surface Effects on the Mechanical Properties of Nanoporous Materials," Nanotechnology, 22(26), p. 265714.
- [14] Feng, X.-Q., Xia, R., Li, X., and Li, B., 2009, "Surface Effects on the Elastic Modulus of Nanoporous Materials," Appl. Phys. Lett., 94(1), p. 011916.
- [15] Briot, N. J., and Balk, T. J., 2015, "Developing Scaling Relations for the Yield Strength of Nanoporous Gold," Philos. Mag., 95(27), pp. 2955–2973.
- [16] Ke, H., Jimenez, A. G., Da Silva, D. A. R., and Mastorakos, I., 2020, "Multiscale Modeling of Copper and Copper/Nickel Nanofoams Under Compression," Comput. Mater. Sci., 172, p. 109290.
- [17] Ke, H., Jimenez, A. G., and Mastorakos, I., 2019, "A Multiscale Approach to Predict the Mechanical Properties of Copper Nanofoams," MRS Adv., 4(5-6), pp. 293–298.
- [18] Deshpande, V. S., and Fleck, N. A., 2000, "Isotropic Constitutive Models for Metallic Foams," J. Mech. Phys. Solids, 48(6), pp. 1253–1283.
- [19] Hanssen, A. G., Hopperstad, O. S., Langseth, M., and Ilstad, H., 2002, "Validation of Constitutive Models Applicable to Aluminium Foams," Int. J. Mech. Sci., 44(2), pp. 359–406.

- [20] Kim, C.-E., Rahimi, R. M., and Bahr, D. F., 2020, "The Structure and Mechanical Properties of Cu 50 Ni 50 Alloy Nanofoams Formed via Polymeric Templating," MRS Commun., 10(2), pp. 286–291.
- [21] Blair, G. W. S., Hening, J. C., and Wagstaff, A., 1939, "The Flow of Cream Through Narrow Glass Tubes," J. Phys. Chem., 43(7), pp. 853–864.
- [22] Gunkelmann, N., Rosandi, Y., Ruestes, C. J., Bringa, E. M., and Urbassek, H. M., 2016, "Compaction and Plasticity in Nanofoams Induced by Shock Waves: A Molecular Dynamics Study," Comput. Mater. Sci., 119, pp. 27–32.
- [23] Gunkelmann, N., Bringa, E. M., and Rosandi, Y., 2018, "Molecular Dynamics Simulations of Aluminum Foams Under Tension: Influence of Oxidation," J. Phys. Chem. C, 122(45), pp. 26243–26250.
- [24] Plimpton, S., 1995, "Fast Parallel Algorithms for Short-Range Molecular Dynamics," J. Comput. Phys., 117(1), pp. 1–19.
- [25] Daw, M. S., Foiles, S. M., and Baskes, M. I., 1993, "The Embedded-Atom Method: A Review of Theory and Applications," Mater. Sci. Rep., 9(7), pp. 251–310.
- [26] Daw, M. S., and Baskes, M. I., 1984, "Embedded-Atom Method: Derivation and Application to Impurities, Surfaces, and Other Defects in Metals," Phys. Rev. B, 29(12), pp. 6443–6453.
- [27] Voter, A. F., and Chen, S. P., 1986, "Accurate Interatomic Potentials for Ni, Al and Ni3AI," MRS Online Proceeding Library, 82, p. 175.
- [28] Xu, H., and Li, Q., 2017, "Effect of Carbon Nanofiber Concentration on Mechanical Properties of Porous Magnesium Composites: Experimental and Theoretical Analysis," Mater. Sci. Eng. A, 706, pp. 249–255.
   [29] Cebeci, H., Stein, I. Y., and Wardle, B. L., 2014, "Effect of Nanofiber Proximity
- [29] Cebeci, H., Stein, I. Y., and Wardle, B. L., 2014, "Effect of Nanofiber Proximity on the Mechanical Behavior of High Volume Fraction Aligned Carbon Nanotube Arrays," Appl. Phys. Lett., 104(2), p. 023117.
- [30] Zhao, M., Schlueter, K., Wurmshuber, M., Reitgruber, M., and Kiener, D., 2021, "Open-Cell Tungsten Nanofoams: Scaling Behavior and Structural Disorder Dependence of Young's Modulus and Flow Strength," Mater. Des., 197, p. 109187.
- [31] Guo, X., Liang, W., and Zhou, M., 2009, "Mechanism for the Pseudoelastic Behavior of FCC Shape Memory Nanowires," Exp. Mech., 49(2), pp. 183–190.
- [32] Cao, A., 2010, "Shape Memory Effects and Pseudoelasticity in Bcc Metallic Nanowires," J. Appl. Phys., 108(11), p. 113531.
- [33] Abdolrahim, N., Mastorakos, I. N., and Zbib, H. M., 2010, "Deformation Mechanisms and Pseudoelastic Behaviors in Trilayer Composite Metal Nanowires," Phys. Rev. B, 81(5), p. 054117.
- [34] Phillips, A., and Sierakowski, R. L., 1965, "On the Concept of the Yield Surface," Acta Mechanica, 1(1), pp. 29–35.
- [35] Gubicza, J., Jenei, P., Nam, K., Kádár, C., Jo, H., and Choe, H., 2018, "Compressive Behavior of Cu-Ni Alloy Foams: Effects of Grain Size, Porosity, Pore Directionality, and Chemical Composition," Mater. Sci. Eng. A, 725, pp. 160–170.